



## A Hand-Based Biometric Verification System Using Ant Colony Optimization

Nirmal Pandey<sup>1</sup>, Prof O.P. Verma<sup>2</sup>, Dr Amioy Kumar<sup>3</sup>

<sup>1</sup>Department of Computer Science & Engineering

Delhi Technological University

New Delhi – 110042

<sup>2</sup>Principal G B Pant Engineering College,

Govt. Of NCT of Delhi, Okhla

New Delhi – 110020

<sup>3</sup>Formerly Guest Faculty (Department of Computer Science & Engineering)

Delhi Technological University

New Delhi – 110042

### Abstract

This paper presents a novel personal authentication system using hand-based biometrics, which utilizes internal (beneath the skin) structure of veins on the dorsal part of the hand and the outer shape of the hand. The hand-vein and the hand-shape images can be simultaneously acquired by using infrared thermal and digital camera respectively. A claimed identity is authenticated by integrating these two traits based on the score-level fusion in which four fusion rules are used *for the integration*. Before their fusion, each modality is evaluated individually in terms of error rates and weights are assigned according to their performance. In order to achieve an adaptive security in the proposed bimodal system, an optimal selection of fusion parameters is required. Hence, Ant Colony Optimization (ACO) is employed in the bimodal system to select the weights and also one out of the four fusion rules optimally for the adaptive fusion of the two modalities to meet the user defined security levels. The databases of hand-veins and the hand-shapes consisting of 150 users are acquired using the peg-free imaging setup. The experimental results show genuine acceptance rate (GAR) of 98% at false acceptance rate (FAR) of 0.001% and the system has the potential for any online personal authentication based application.

**Index Terms:** Biometric Authentication, Infrared thermal vein patterns, hand-shapes, Score-level fusion, ACO.

### I. INTRODUCTION

Biometric based personal authentication is aimed at determining the claimed identity based on user's physiological/behavioral traits [1]. The biometric authentication system utilizes stepwise procedures. In the first step, a sensor acquires the biometric modality which is converted into the digital image. In the second step, the feature extraction module extracts the reliable features from the digital image and a data storage component saves the biometric feature templates corresponding to each enrolled user. In the third step, the matching module compares the test biometric template with the training templates and provides both the genuine and imposter matching scores. In the fourth step, the decision module acts upon the matching scores to learn a decision threshold between the genuine (acceptance) and the imposter (rejection) for the claimed

identity [1]. A conventional way to choose the best decision-threshold to improve the performance is via Receiver Operating Characteristics Curve (ROC) which is a plot of false acceptance rate (FAR) vs. false rejection rate (FRR) [1]. The mode of authentication in a biometric system can be categorized into two types: identification and verification. Identification is the 1: N match obtained by matching the test pattern with each of the enrolled patterns. The unknown identity can be traced out by providing the best match among  $N$  matches [1]. The verification is a 1:1 whereby the claimed identity of a pattern is verified by matching it with the enrolled patterns. If the user identity is unknown, the authentication can only be performed under the identification mode [11]-[14]. When the user's identity is known, verification is the most preferred mode for the personal authentication [6]-[10]. This paper presents a novel hand based bimodal system using hand veins and hand shape for biometric based verification. It is designed to adaptively select the fusion parameters according to the desired security requirements.

### **A. Hand-Based Bimodal System**

Hand-based biometrics, particularly palmer part has been studied extensively in the recent years and many authentication systems are developed using fingerprint [2]-[4], palmprint [5]-[7] and hand-geometry [8]-[9] with high user acceptance. However, being the outer most part of the human body people leave their fingerprints and palm impressions unconsciously. This sort of negligence is prone to security risks on these modalities.

The slowly gaining popularity of the vein patterns as a promising biometric trait for the personal authentication is due to its ability to defy imposter attacks. The veins being the blood carrying vessels are a part of the vascular system of the body and any change in the body generally affects the vascular system. Normally, it expands with the growth of the body from the childhood and remains fairly stable between 16 to 60 years of age. The vein patterns of persons lying within this age group can serve as a unique biometric. Located beneath the skin, vein patterns are difficult to spoof by an imposter attack, and hence are a safer biometric trait. But then, being a hidden structure of the human body, the acquisition of vein patterns are highly susceptible to environmental conditions like ambient temperature and humidity [10]. Therefore, the need is to make a bimodal system where the vein patterns can be integrated with other biometric traits.

In this work, a bimodal system is developed using vein patterns extracted from the dorsal part of the hand and the contour information from the same part of the hand, called as *hand-shape*. The infrared thermal camera is used to capture hand-vein patterns while visible light camera is used to acquire hand-shape images. Both the biometric traits can be simultaneously extracted from the claimed identity and integrated before final accept/reject decision. The objectives of this bimodal system are: (i) To improve the overall performance, (ii) to increase the system accuracy, and (iii) to withstand imposter attacks whenever deployed for the personal authentication.

### **B. The Bimodal System Using ACO**

The widely used strategies for the fusion of two modalities in a bimodal systems are score-level fusion [11] and the decision-level fusion [11]. A typical multi biometric system requires the fusion parameters such as the selection of the decision- thresholds corresponding to each modality and a fusion rule for their integration. The selection of these parameters depends upon the desired security requirement which can be expressed in terms of the two error rates: FAR and FRR. The choice of acceptable error rates is application dependent. For example, the high security applications (e.g., access to a building, or to a bank account) require the lowest possible

FAR (close to zero) but a permissible value of FRR to prevent false authentication (imposter) whereas the low security applications (e.g., public transport, classroom access) can be managed with somewhat high FAR but FRR must be stringent, i.e. as low as possible. The homeland security department envisages such a multi level security requirement in view of the forensic, civilian and high security applications within the purview of the color-coded terrorism threats [12].

However, most of the bimodal systems available in the literature [2]-[9] offer fixed level of security involving a fixed number of fusion parameters for the desired level of accuracy. The security provided by these biometric authentication systems is not adaptive to cater to the wide ranging applications requiring multiple levels of security [13]. Therefore, the need arises for an adaptive bimodal system capable of selecting the optimal fusion parameters to achieve the desired level of security. Hence an optimization approach is needed to guide the search for the optimum parameters. Some of the approaches for searching the optimal parameters can be categorized as: Deterministic methods [14], Probabilistic methods [15], and Evolutionary methods [16]. In comparison to other search algorithms, Evolutionary Computation (EC) techniques [16] generate a set of relevant solutions, termed as *population* and then find an optimal solution by searching and updating the memories (i.e. the past history of the particles) of the population. The techniques, such as Genetic Algorithm (GA) [16], Particle Swarm Optimization (PSO) [17], Ant Colony Optimization (ACO) [18], Bacteria Foraging (BF) [16] are generally influenced by the social behavior of species such as birds, fish, ants, bacteria, etc.

The advantages of the evolutionary computation include that it is easy-to follow, robust to changing circumstances, and flexible. Further, most of the evolutionary techniques provide a global solution which may not be the case with the optimization techniques which give the local optima. Evolutionary techniques can be applied to those real world problems for which the heuristic algorithms can lead to unsatisfactory results. Thus, the use of the evolutionary techniques is gaining immense popularity, particularly for the real life problems. This paper presents a novel bimodal system having the hand-veins and the hand-shapes as its two biometric modalities and employs ACO for selecting the fusion parameters of this system for meeting varying security levels.

The paper is organized as follows: a few state of the art methods on the bimodal/multimodal systems are presented in Section II. The image acquisition and the normalization of both the modalities are briefed in Section III while the feature extraction is described in Section IV. The fusion methodology of the bimodal system using ACO is discussed in Section V. The experimental results and a relevant discussion are relegated to Section VI and VII respectively. Finally, the conclusions are given in Section VIII.

## II. THE STATE OF THE ART

### A. *The Prior Works*

The fusion of multiple biometrics in a multimodal system can be broadly categorized into two stages: (1) *fusion prior to matching*, which includes *sensor level* and *feature level* fusion schemes and (2) *fusion after the matching*, which can be performed at both the *score level*, and *decision level*. Though the extracted biometric features have rich information on the biometric data, the fusion schemes cause the deterioration of performance due to the loss of information at each level of fusion [1] [11]. As compared to the fusion prior to matching, the fusion after matching is not entangled with the issue of incompatibility. Hence, either the score level or the decision level

fusion scheme is preferred over the sensor level or the feature level fusion scheme in the multimodal biometric systems [11].

The history of bimodal/multimodal systems is more than a decade long and various developments have taken place during this period. Hong et al. [19] have proposed a bimodal system using fingerprint and face in 1998. They have fused the Eigen faces and the minutiae features from fingerprints at the decision-level to achieve FRR of 6.6% and FAR of 0.01% in comparison to FRR of 61.2% for face and 10.6% for fingerprint at the same FAR. Frischholz et al. [20] have presented probably the first commercial system BioID using lip movement and face images extracted from the same video sequence. They have achieved equal error rate (EER) of below 1% by their system. In the development of a multimodal biometric system, Fierrez et al. [21] have fused fingerprint, face, and signature. Using the three fusion schemes, viz., sum rule, user-independent SVM and user-dependent SVM, they achieve EERs of 0.5%, 0.3%, and 0.005% respectively. But without fusion the individual EERs are rather very high, i.e. 3%, 4% and 10% on fingerprint, face and signature respectively.

Kumar et al. [22] have come up with a bimodal system consisting of two biometric modalities, palmprint and hand-geometry. They have undertaken two types of fusion one at the feature level and other at the score-level. Their bimodal system yields FAR of 0% at FRR of 1.41% with the score-level fusion. Ross et al. [23] have attempted at a multimodal system using fingerprint, hand-geometry, and face as its constituent modalities. They have compared three fusion approaches: sum rule, decision tree, and linear discriminant function on their multimodal system. The sum rule is shown to give FAR of 0.03% at FRR of 1.78% while the fingerprint alone leads to FAR of 0.01% at FRR of 25%. Jain et al. [24] have proposed another multimodal system using fingerprint, hand-geometry, and face biometrics. They achieve FAR of 0.1% at FRR of 1.4% on the multimodal system whereas fingerprint is alone found to offer FAR of 0.1% at FRR of 6.4%.

From the above we conclude that the bimodal/multimodal systems are surpassing over the unimodal systems in terms error rates. However, most of them offer a fixed level of security with a fixed number of fusion parameters. On the other hand, a biometrics-based multimodal system should be adaptive to cater to the wide ranging applications requiring multiple levels of security [13]. An adaptive bimodal/multimodal [25-26] biometric system is relatively new advancement and is of particular interest to the present work. Kalyan et al. [25] have presented an adaptive multimodal biometric system where they consider 16 binary decision rules arising from the two participating sensors and adaptively select one rule using binary PSO. In another approach for an adaptive multimodal system, Kumar et al. [26] have adopted the score-level fusion with four fusion rules; two of which are linear (sum and product) and the rest two are non-linear (exponential-sum and Tanh). They have implemented these rules on three bimodal systems consisting of i) palmprint and iris; ii) face and speech; and iii) fingerprint and hand-geometry. The performance of the score level fusion with their rules is shown to be better than that reported in [20]. However, both [25] and [26] utilize PSO to learn the fusion parameters.

### *B. The Motivations*

The survey on bimodal/multimodal authentication systems [2]-[9] shows that most of bimodal/multimodal systems do not meet the varying security requirements [13]. Further, the hand-based biometrics such as fingerprint and palmprint, though possess significant details yet they are prone to imposter attacks as people leave their hand marks wherever they touch. These two multimodal systems in the literature [25-26], which offer an adaptive security, use PSO for

the optimal selection of the fusion parameters. The PSO algorithm has its own limitations like ending up in the local minimum leading to the premature convergence [27] and is applicable to the continuous domain. Further, the sigmoid function used to convert the continuous PSO into the binary PSO in [25][26] is a discrete variant of PSO which approximates the velocity and the position updates of each particle. Going in for a direct discrete domain evolutionary technique is certainly advantageous in place of the discrete variants of PSO. Thus there is a need to explore other evolutionary techniques for adaptive security. In this context, Bacterial foraging [18] that has a mechanism to decide the direction for the optimal solution may seem useful. However, the foraging strategies involve a large computation in four stages: *chemotaxis*, *swarming*, *reproduction*, and *elimination and dispersal* to reach upon an optimal solution. Hence they are not well suited for online biometric applications where quick decisions are of primary concern. Similarly genetic algorithm [28] has several misgivings like an expensive fitness function, convergence to local minimum, and prospectus of divergent solutions on dynamic datasets. We therefore, use ACO for the selection of fusion parameters in the proposed bimodal system.

### C. The Proposed Approach

Despite the current popularity of the hand-vein patterns as a promising biometric trait [10][29]-[31], they are rarely used in bimodal/multimodal systems. This motivates us to develop an adaptive bimodal system incorporating the hand-vein patterns and hand-shapes that possess the contour information on the dorsal part of the hand. An attempt is already made in the creation of a bimodal system comprising hand-veins and the palmprints [32] based on the decision-level fusion facilitated by ACO. However, our preference to hand-shapes over palmprints is due to its touchlessness and less chances of imposter attacks. The block diagram of the bimodal authentication system is shown in Fig. 1.

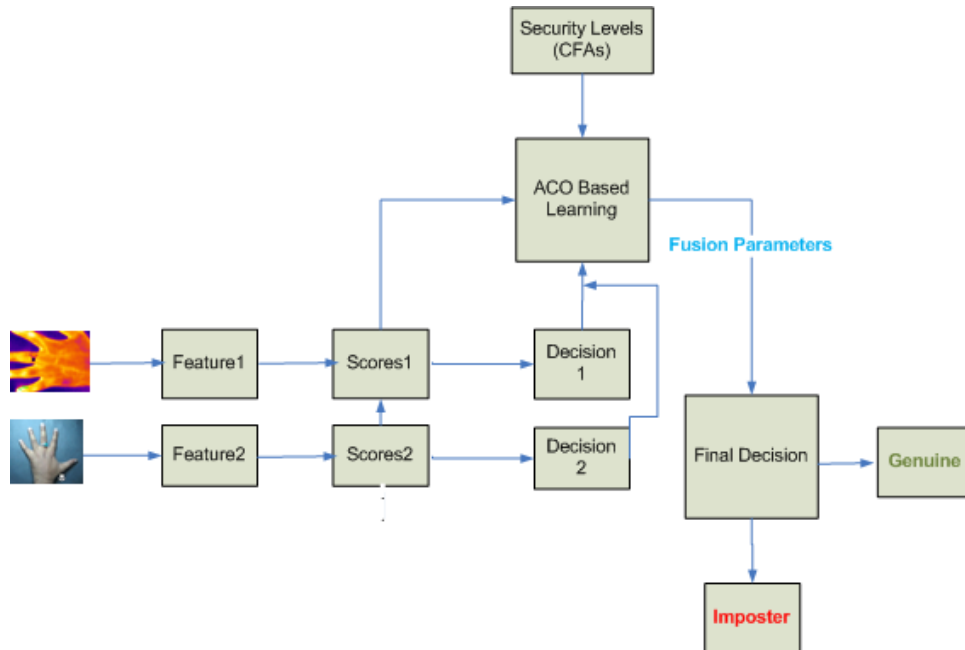


Fig. 1 Block diagram of the ACO-based adaptive bimodal system

### The three-fold contributions of our work are now elaborated here:

1. Proposition of a bimodal system by fusing hand-vein patterns with the hand-shape at the score-level. The infrared thermal camera is used for the acquisition of vein patterns and

an ordinary digital camera for hand-shape. The Radon transform the linear trends in an image by aggregating the intensities along all possible lines [33]. The transform is used here for extracting features from the hand-vein patterns. The Independent Component Analysis (ICA) based appearance features are extracted from the hand-shapes [34]. The claimed identity is authenticated by fusing the scores computed from these two traits.

2. Utilization of ACO for the bimodal system adaptive to various civilian and forensic applications [13]. ACO has been utilized in earlier approaches for fusion in multispectral palmprints [35], feature selection in face images [36], and our earlier work on fusion of hand-vein and palmprints [32]. Note that in ACO, after updating the pheromone levels, the conventional way is to choose new paths for the next iteration from the complete set of candidate solutions. However, instead of trying out all candidate solutions, the ones with low probability can be discarded. This narrows down the search space and improves the quality of paths chosen by ants. Hence, the probability of selecting the next solution is constrained to lie between the lower and the upper values determined from the current local and global solutions. In this work, a framework is developed using the local and global updates carried out in ACO. This framework is then used for the optimal selection of fusion parameters in the bimodal system devised using hand-vein and hand-shape.
3. A comparison of the two scenarios of adaptive multimodal fusion. We first compare the ACO-based selection of fusion parameters with the PSO based ones in our bimodal system. We find ACO-based bimodal system yields lower error rates than that of PSO. The score-level fusion methodology in ACO is also compared with the decision-level fusion approach and is found superior to it in the selection of the fusion parameters.

### III. IMAGE ACQUISITION AND NORMALIZATION

#### A. Vein Images

The vein patterns located beneath the skin on the dorsal part of the hand are not visible in the ordinary light while hair, moles, warts, etc, on the skin hinder an accurate acquisition by an ordinary digital camera. Further colors and attributes of fat/thick skins reduce the visibility. The acquisition is done at the indoor temperature in the range of 10<sup>0</sup>C- 30<sup>0</sup>C and at the relative humidity of 25%-50% as per the weather conditions. The visibility of the thermal imaging is affected at the outdoor environment and in such conditions segmentation of the vein patterns from background is very difficult [30]. Even when the images are acquired indoor, the visibility is sometimes affected due to sudden change in the temperature like: when a user leaves the outdoor environment to enter the indoor environment for imaging. To counter the above situation, we wait for a few seconds for the operating conditions to be restored before starting the acquisition again. The imaging setup and the acquired image are shown in Fig. 2.

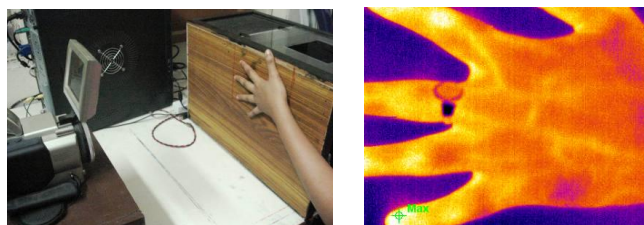


Fig.2. (a) Camera Setup (b) Captured Image

The images are acquired from the peg-free set up where the user's hand movement is not

constrained by pegs and the ROIs are made invariant to rotation and translation. An algorithm is devised to extract Region of Interest (ROI) of vein patterns by fitting a coordinate system on the palm dorsa. The ROI extraction method, somewhat similar to [31], is as follows:

1. To determine the webbing between the fingers, the images are binarized. A histogram-based binarization method is utilized to choose the appropriate threshold from the captured images. By analyzing the bimodal property of the histogram of the dorsa images, local maxima P1 and P2 can be pinpointed and the local minimum T between them is determined. This local minimum becomes a threshold to segment the image. The input image and the corresponding histogram are shown in Fig. 3. Fig. 4 (a)-(b) shows the binarization using both the normal method and the histogram-based method.

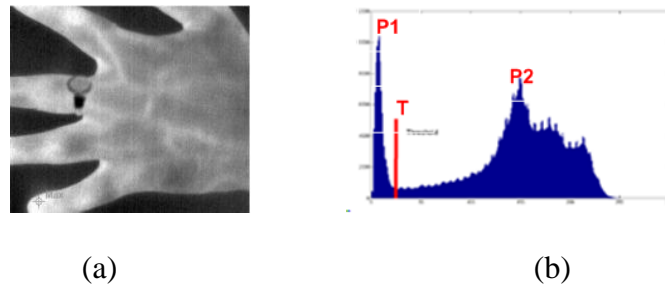


Fig. 3 (a) Vein image (b) Histogram of Image

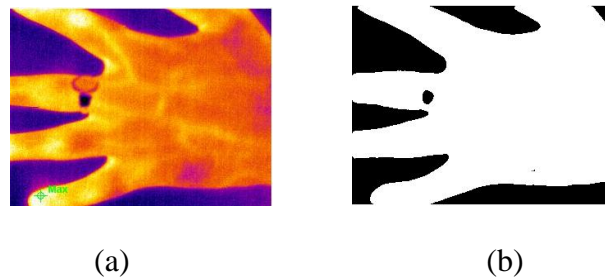


Fig. 4 (a) The acquired thermal image (b) The binarized image from histogram method

2. From the binarized image, a closed boundary is traced out in the clockwise direction. Moore-Neighbor tracing algorithm modified by Jacob's stopping criteria [44] is used for tracing the boundary points from the binarized image. The boundary points are then used for computing the tips and valleys of the hand by taking the bottom-left point marked  $P_s$  as the starting point and the middle point marked as  $W_m$  {Shown in Fig. 5 (a)}. We calculate the Euclidean distances between  $W_m$  and the boundary points  $P_s$ . The distances start increasing while tracing the boundary clockwise till the tips of the finger marked as point of local maxima are reached. These distances then start decreasing when calculated with the points way from the fingertips till the valleys of the same finger marked as local minima are reached. As evident from Fig. 5 (a) the distances are constant for a few boundary points (Represent the boundary of the fingertip) before start decreasing. We consider the midpoint of these points as tip of the finger. The valley point is the local minima. Similarly, five tips and four finger valleys are determined as shown in Fig. 5 (b).

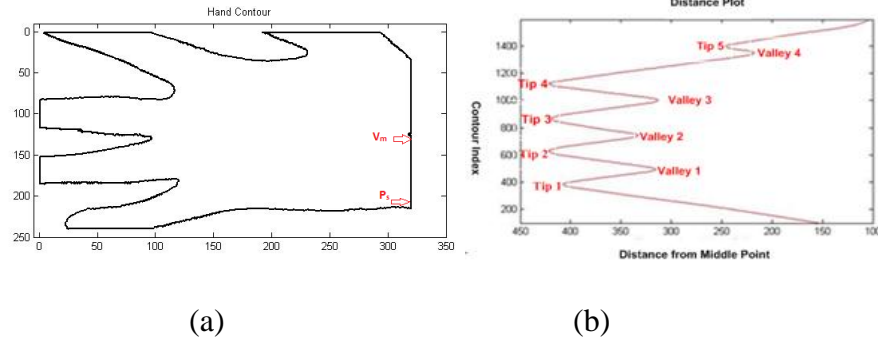


Fig. 5 (a) The boundary extracted from the hand contour (b) Tips and valleys of the hand

3. A tangent is drawn between the second and the fourth finger-valleys forming a line R1-R2. The middle point of this line is taken as the reference point and a perpendicular distance from this point decides the length of the square region {See in Fig. 6 (a)} with corners at R1, R2, R3 and R4. This square region is finally cropped and saved as ROI (See in Fig 6 b).

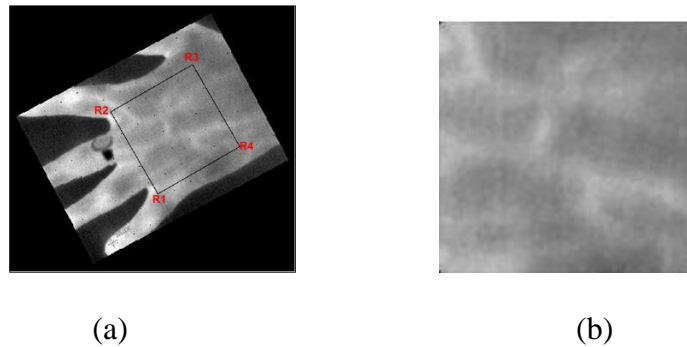


Fig. 6 (a) Located ROI area on Palm dorsa (b) Extracted ROI

### B. Hand Images

The images on the dorsal part of the hand are acquired using Canon A630 digital camera. A wooden box is made with an open cut on its upper part to fix the camera on it. The inner side of the box is meant to place a user's hand. The setup has a ring shaped fluorescent tube fixed under the roof of the box. The use of pegs and extra-illumination is avoided for ease of acquisition. The camera is focused on the dorsal part of the hand to capture the details. However, users are requested to place the hand in a marked place in order to keep it in the focus of the camera. The imaging setup and acquired image are shown in Fig. 7.



Fig. 7 The Hand Image (a) The Camera Setup (b) The Captured Image

The tips and valleys from the acquired hand-shape help in the separation of the fingers from the hand. The separated fingers are rotated with respect to the pivotal axis formed by their vertices and the final hand contour is extracted by stitching them back to the wrist part [29]. The steps of the normalization are as follows:

1. The hand image is segmented from its background. As there is no extra light, the illumination management is applied; the acquired hand images are too difficult to be segmented by thresholding. Hence, a novel skin detection-based segmentation method is developed. In this, the red ( R), green (G) , and blue (B) components of the image are made use of as under:

*Calculate*

$$Sum=R+G+B \quad (1)$$

$$R\_percent=R/ Sum \quad (2)$$

$$G\_percent=G/Sum \quad (3)$$

$$B\_percent=B/Sum \quad (4)$$

*If*

$$\{ R\_percent, G\_percent, B\_percent \} \in [30, 40]$$

*The pixel is on the skin*

*Else*

*The pixel is on the background*

After the skin detection, the image is binarized by making the skin surface white, while the background as black. The binarized image is then filtered to get the clean image. The original image and the binarized image are shown in Fig. 8 (a) and 8(b) respectively.

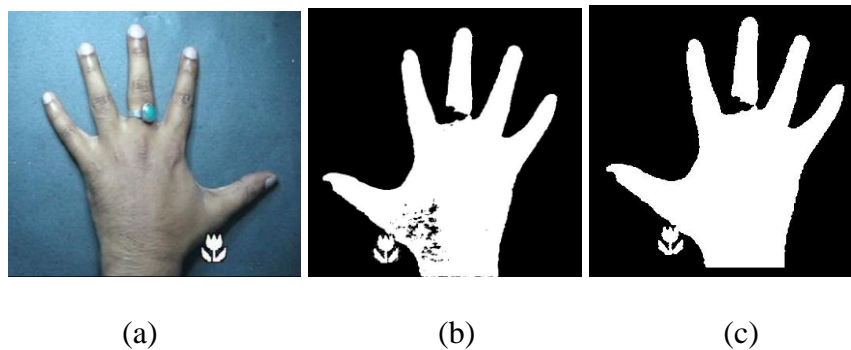


Fig. 8 Segmentation of the hand images: (a) The original image (b) The segmented by skin detection (c) The filtered image

- The operations involving the separation of the fingers, rotation along the pivotal axis and stitching of the fingers to the wrist to get the normalized hand contour image are the same as in [34]. Fig. 9 shows these operations.

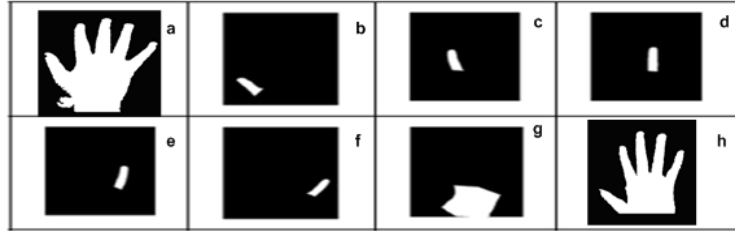


Fig. 9 Normalization of the Hand Image: (a) The binarized hand image (b)-(g) fingers and wrist separated from the hand image (h) The normalized hand-shape contour.

#### IV. FEATURE REPRESENTATIONS

##### A. Vein Features

The vein patterns possess enough texture details that serve as feature representation. One kind of texture features arise from the principal lines that can be used for matching two vein images. However, the vein patterns in our database are full of wrinkles which are small lines caused due to noisy acquisition; hence should be separated out from the principal lines before matching. The separation can be done by noting that the line energy on the principal lines is stronger than on wrinkles. Radon transform is used for detecting the directions of the principal lines and the energies in the vein patterns.

A straight line can be represented either in the slope-intercept form,  $y=ax + b$  in Cartesian co-ordinates, or by normal representation,  $x \cos \theta + y \sin \theta = \rho$  in the polar co-ordinates. Here  $\rho$  is the perpendicular distance from the origin and  $\theta$  is the angle between the line and the  $y$ -axis. The Radon transform of a 2D function  $f(x, y)$  is a line integral along an arbitrary line in the  $xy$ -plane [37]. Copeland et al. [43] have presented a modified Radon transform to detect line segments in the local areas which are significantly shorter than the image dimensions by redefining the transform as:

$$Rad(r, \theta) = \int_{y_{\min}}^{y_{\max}} \int_{x_{\min}}^{x_{\max}} f(x, y) \times (x \cos \theta + y \sin \theta) dx dy \quad (5)$$

The parameters:  $x_{\max}$ ,  $x_{\min}$ ,  $y_{\max}$ , and  $y_{\min}$  define a local area to perform Radon transform in (5). Radon based enhancement has also been implemented in [33] for extracting palmprint principal lines and in [37] for image representation. The approach of Matus et al. [37] utilizes the Radon transform for the finite length signals by the summing of the image pixels over a certain set of lines. The approach in [33] makes use of [37] for detecting the palm lines by modifying it using modulo operation to reduce the “wrap around” effect. Our implementation of Radon transform for vein patterns is similar to that in [37] for palmprints. They have modified the Radon transform for the real function  $f[x, y]$  by denoting a group  $\{Z_p = 0, 1, \dots, p-1\}$ , where  $p$  is a prime number defined as:

$$Rad_f(k) = \frac{1}{C} \sum_{(i,j) \in L_k} f(i,j) \quad (6)$$

Where  $C$  is a scalar to control the scale of the transform, and  $L_k$  denotes a set of points constituting a line belonging to  $Z_p^2$  as:

$$L_k = \{(i, j) : j = k(i - i_0) + j_0, i \in Z_p\}, 0 \leq k \leq p \quad (7)$$

Where  $(i_0, j_0)$  denotes the centre point of  $Z_p^2$ , and  $k$  indicates the slope of  $L_k$ . Here,  $Z_p^2$  can be thought of a local window in the vein ROI and  $L_k$  denotes a set of points extracted as principal lines from  $Z_p^2$ . We have another notation for  $L_k$  as  $L(\theta_k)$  which represents the direction image and is calculated from:

$$\theta_{k(i_0, j_0)} = \arg(\min_k (Rad_f(k))) \quad (8)$$

$$\text{Energy}_{(i_0, j_0)} = (\min_k (Rad_f(k))) \quad (9)$$

For ROI of size  $m \times n$  (Fig. 6 (b)), the centre of the window  $Z_p^2$  ( $p=17$  in our case) moves from pixel to pixel. The energy image and the principal line image resulting from applying Eqn (9) and Eqn. (7) [33] are shown in Fig. 10 (b)-(c). These images are combined to give an enhanced vein pattern image, shown in Fig. 8 (d) which is matched using the normalized Hamming distance by generating the matching scores.

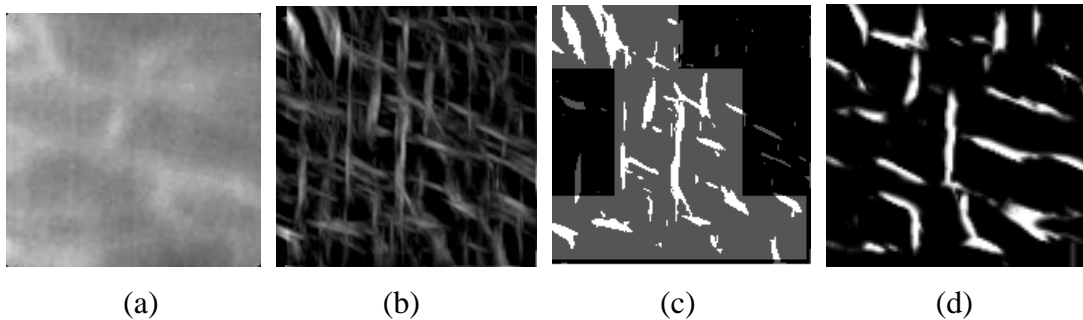


Fig. 10 (a) The Original ROI (b) Energy image (c) Principal line image (d) The Enhanced ROI

### B. Hand-shape Features

The normalized hand-shapes (See Fig. 9) contain the contour information of the hand dorsal part. As the contour images have no textural or line details (as in the case of fingerprint or palmprint) it can be best represented by appearance features, which are obtained by the application of principle component analysis (PCA). However, as shown in [38] that the independent component analysis (ICA) is more robust and well suited as appearance features which have been applied to hand [34] and face [38] biometrics. In this work, the appearance features are extracted from hand-shape images by applying ICA which decomposes a mixed signal into the additive subcomponents of the non Gaussian type [39]. The dependencies in the hand-shape images need to be separated into independent components to obtain as ICA features. The theory and implementation of ICA is explained in [39]. The detail of ICA features is now in order.

The ICA model considers a hand-shape image as a combination of independent components (ICs) and a mixing matrix. Let  $X_{K \times N}$  be the a hand-shape image,  $M_{N \times N}$  be the mixing matrix and  $C_{K \times N}$  be the matrix of ICs, these bear a relation:

$$X_{K \times N} = C_{K \times N} \times M_{N \times N} \quad (10)$$

The task in ICA is to estimate the independent components from the input image as:

$$C = X \times (M^{-1}) \quad (11)$$

Here, determining  $C$  from  $X$  is known as Blind Source Separation because the input source has to be separated into independent components without any knowledge of the mixing matrix. Though there are several approaches for the estimation of ICs from Eqn (10), we have considered the FastICA algorithm [39] that maximizes the statistical independence between the output components using maximization of the negentropy.

We have used here a hand-shape database of 150 users with 5 samples each. Each of the hand-shape images is of size  $150 \times 150$ . The mean-sample image for each user is computed by taking the average of 5 enrolled samples images. The mean-sample image is resized to get a image vector of size  $22500 \times 1$ . The mean-sample image is computed for all 150 users and the image matrix  $X_{22500 \times 150}$  where  $K=22500$  and  $N=150$ . As  $X$  is found to be of high dimensions, PCA is first employed on  $X$  for the dimensionality reduction. Let  $U_{22500 \times 150}$  be the projection (eigenvector) matrix and  $Mean_{22500 \times 1}$  is the mean vector arising from the application of PCA on  $X$ . The image matrix  $X$  is then transformed by PCA to get the projection matrix  $Y_{150 \times 150}$  as follows:

$$Y_{150 \times 150} = (X_{22500 \times 150})^T \times U_{22500 \times 150} \quad (12)$$

By applying the FastICA algorithm on projected matrix  $Y$  we obtain the IC matrix  $C_{150 \times 150}$  using Equations (10) and (11). At the verification/identification stages, let  $Q_{22500 \times 1}$  be the image matrix computed from input hand-shape image. Subtracting the mean vector  $Mean_{22500 \times 1}$  from it leads to

$$Vector1_{14400 \times 1} = Q_{22500 \times 1} - Mean_{22500 \times 1} \quad (13)$$

Multiplying the Vector1 with the PCA projection matrix gives the Eigen feature vector as:

$$Eigenfeature_{1 \times 150} = Vector1_{22500 \times 1}^T \times U_{22500 \times 150} \quad (14)$$

Use of the IC matrix on the Eigenfeature vector yields the ICA feature vector as:

$$ICAfeature_{150 \times 1} = B_{150 \times 150} \times Eigenfeature_{1 \times 150}^T \quad (15)$$

Here the Euclidean distance is used to match two ICA feature vectors. Let  $ICAV_1$  and  $ICAV_2$  be the two ICA features computed using Eq. (15). The matching score  $s$  between these two vectors is computed as:

$$s = \sqrt{\sum_{i=1}^{150} \{ICAV_1(i) - ICAV_2(i)\}^2} \quad (16)$$

## V. ACO-BASED FUSION

### A. Adaptive Bimodal management

In the proposed bimodal system, an optimal selection of fusion strategies along with the associated fusion parameters for meeting the multiple levels of the security requirements.

Decision-threshold and a fusion rule are the two basic *fusion parameters* that need to be selected optimally. The performance of a typical biometric system can be evaluated in terms of the error rates: FAR and FRR. One way of ensuring different security levels is to assign different costs to these error rates and study the fusion parameters for each security level. If high security is required, the cost of FAR can be chosen much higher than that of FRR; as in this case an imposter acceptance should be as less as possible. But, in the case of low security, the cost of FRR is higher than FAR; as in this case the genuine rejection is required to be as less as possible. Therefore, different security levels in a multimodal system can be enumerated by using the cost of false acceptance (CFA) and cost of false rejection (CFR). Both costs can belong to [0, 1] in the step size of 0.1 providing us with 20 discrete points which represent the different security levels. The fusion parameters need to be computed for each security level by employing error rates of the individual biometrics and the allowable fusion rules. The overall error (also our objective function) can be computed by taking both the costs as the weights to the FAR and FRR in the following:

$$G = CFA \times FAR + CFR \times FRR \quad (17)$$

Where  $CFA + CFR = 2$

The FAR and FRR are the outcome of applying a decision-threshold ( $\alpha$ ) on the matching scores [26]. Four score-level fusion rules: Sum, Product, Exponential Sum and Tan-hyperbolic (Tanh) Sum are considered for fusion at the matching score-level as in [26]. Let  $s_j$  be the matching scores from  $j^{\text{th}}$  modality and  $W_j$  be the corresponding weight, where  $j=1, 2$  for two modalities. The fusion rules for aggregating the matching scores are chosen as:

$$Sum = \sum_{j=1}^2 s_j W_j \quad (18)$$

$$Product = \prod_{j=1}^2 s_j^{W_j} \quad (19)$$

$$Exponential Sum = \sum_{j=1}^2 \exp(s_j) W_j \quad (20)$$

$$Tanh Sum = \sum_{j=1}^2 \tanh(s_j) W_j \quad (21)$$

Here, weights are selected according to the security levels for the adaptive fusion of the vein patterns and the hand-shape biometrics. The inputs to the ACO are: the security levels, the weights corresponding to both the modalities; and the four score-level fusion rules {Equations (18)-(21)}. The outputs of the ACO are: a decision-threshold, optimal weights corresponding to each modality, and a fusion rule. The task of ACO is to minimize the overall error  $G$  (Eq. 17) by selecting the weights for each modality and a fusion rule.

The population in ACO is initialized in the  $D$ -dimensional space. An ant can be represented as  $X_{md} = (x_{m1}, x_{m2} \dots x_{mD})$ , where the first subscript  $m$  represents a  $m^{\text{th}}$  solution, and  $D$  denotes the dimension. For the score-level fusion, each ant has " $N+2$ " dimensions, where  $N$  is the number of modalities which 2 in this work. Thus, out of four dimensions, the first 2 dimensions are meant for the weights ( $W$ ) assigned to each modality, the 3<sup>rd</sup> dimension is kept

for the decision-threshold, and 4<sup>th</sup> dimension represents a fusion rule. An ant thus represents a parameter vector:

$$X_{md} = \{ W_1, W_2, \alpha, F \}, \quad (22)$$

Where  $F$  is one fusion rule chosen from Eqns. (17)-(20).

### B. A Brief Description of ACO

Ant colony optimization (ACO), first introduced by Marco Dorigo, is a class of optimization algorithms applicable to the problems seeking optimal paths [40]. The salient features of ACO include the positive response, circulated computation, and greedy heuristic. The positive response promotes quick search for optimal solutions, the circulated computation removes the premature convergence, and the greedy heuristic assists in searching for desirable solutions at the early stages of the algorithm. The ACO algorithm relies on the pheromone-based probabilities to search for the optimal paths [40]. While searching, the moving ants (probable solutions) deposit some pheromone which evaporates over a trail period on the chosen paths. Any ant encountering a previous trail decides to follow a path having a high concentration of pheromone meaning thereby many ants had already tread that path. As a result, the collective behavior emerging from several trails is a kind of positive feedback for the selection of an optimal path. The pheromone evaporation prevents the premature convergence as no single ant can ever dictate a path; and the selected path is a collective judgment [40].

The ants are initialized as in Eq. (22). Initially, each ant deposits an equal amount of pheromone level. Now, the objective function  $G$  {See Eq. (17)} is evaluated for each ant. The individual weights are applied on the chosen fusion rule to get the fused matching score. The decision-threshold  $\alpha$  is then used to compute FAR and FRR from the fused matching scores incorporating a security level. The updated pheromone level  $\tau_i^{t+1}$  at  $(t+1)^{th}$  iteration where  $i$  denotes the  $i^{th}$  ant is given by

$$\begin{aligned} \tau_i^{t+1} &= \rho \times \tau_i^t + \frac{Q}{G}, \text{ if } i^{th} \text{ ant minimizing the } G \\ &= \rho \times \tau_i^t, \text{ Otherwise} \end{aligned} \quad (23)$$

If any of the ants (newly computed solutions) participates in the minimization of the objective function ( $G$ ), the value of the pheromone level increases by  $Q/G$ ; where  $Q$  is a constant chosen by trial and error in the range [0.005, 0.01]. A value of 0.01 is found to be appropriate here. Along with the update of the pheromone levels, the probability of the  $i^{th}$  ant is computed for the next iterations as:

$$P_i = \frac{\tau_i^{(t)}}{\sum_{k=1}^D \tau_k^{(t)}} \quad (24)$$

The probability of selecting ants which minimizes  $G$  gets better than that of other ants in Eq. (23) in the next iteration where the pheromone levels are comparatively less.

One important parameter of ACO is the evaporation factor ( $\rho$ ) in Eq. (23) that influences the probability in Eq. (24). The ACO suffers from the problem of saturation of the pheromone

level for small values of  $\rho$  (close to 0) forcing the ants stuck on a particular path. On the other hand if  $\rho$  is close to 1, every path will have equal probability with no scope for optimization. To overcome this,  $\rho$  is set to 1 initially and subsequently decreased in steps of 0.005. This strategy not only prevents the ants from being dragged on any non-optimal path but also allows them to navigate to an optimal path. Unlike the traditional ACO where complete search space is used to select the solutions at the next iteration, the search space is constrained by introducing the lower and the upper values, i.e.  $L$  and  $U$ . The local best, the global best, and the current position (denoted by  $A_{lb}$ ,  $A_{gb}$  and  $A_{cp}$  respectively) are calculated for all ants at every iteration. From  $A_{lb}$ ,  $A_{gb}$ , and  $A_{cp}$ ,  $L$  and  $U$  are derived as the limiting values. At the first iteration, an equal amount of pheromone is assigned to all the paths and the probabilities are calculated accordingly. From the next iteration onwards, the probabilities are assigned by modifying (24) as :

$$p_i = \frac{\tau_i^{(t)}}{\sum_{k=L}^U \tau_k^{(t)}} \quad (25)$$

The constraints on  $A_{cp}$ ,  $A_{lb}$  and  $A_{gb}$  that facilitate the option of  $L$  and  $U$  are given in Table 1. The limiting conditions are checked for each ant and the values of  $L$  and  $U$  are decided accordingly.

**Table1:** The Limiting Conditions for the ACO search

Limiting conditions	The value of L	The value of U
$A_{lb} \in ]A_{cp} A_{gb}[$	$A_{cp}$	1
$A_{cp} \in ]A_{lb} A_{gb}[$	$A_{lb}$	1
$A_{gb} \in ]A_{lb} A_{cp}[$	$A_{lb}$	$A_{cp}$
$A_{gb} \in ]A_{cp} A_{lb}[$	$A_{cp}$	$A_{lb}$
$A_{cp} \in ]A_{gb} A_{lb}[$	0.001	$A_{lb}$
$A_{lb} \in ]A_{gb} A_{cp}[$	0.001	$A_{cp}$

### C. The ACO Algorithm

The ACO algorithm is outlined here:

- I. Initialize the population of the ants randomly in the search space (See Section V A). For the score-level fusion, the weights corresponding to each modality are assigned values between 0 and 1.
- II. Specify the pheromone levels of all ants as the discrete array  $(\tau W_1, \tau W_2, \dots, \tau W_p)$  for the score-level fusion. They are fixed at the same pheromone value at the first iteration and the probabilities are computed using Eq. (24).
- III. Update the local and global best positions of the ants as in Section III B and evaluate the probabilities using Eq. (25).
- IV. Iterate until the end of the specified number of iterations.

## VI. EXPERIMENTAL RESULTS

A database of 150 users with 5 samples per user is acquired at the Biometric Research Laboratory, IIT Delhi. The Radon features for the vein patterns and ICA features for Hand-shapes are extracted for all the enrolled samples of each user. Out of 5 enrolled images, 3 samples are chosen for the training and the rest are for the testing. The Euclidean distance is used to match both the Radon and ICA features extracted from vein patterns and hand-shape respectively (See Eq. 15). Some of the conventional performance metrics and the key terms utilized in the proposed bimodal system are elaborated as follows:

- I. *The matching scores:* The training and the testing samples of each user are matched using Euclidean distance to calculate the matching scores. If the training and the testing images belong to the same user, the matching scores are referred to as the *genuine score*, otherwise *imposter scores*. Hence, in case of genuine matching score, all the three training images of a user are matched with first test sample of the same user to compute three matching scores. The minimum of these scores is taken as genuine score from first test sample. Similarly a matching score for another test image is computed for the same user. Hence, for 150 users, 300 genuine matching scores ( $150 \times 2$ ) are computed for both vein patterns and hand-shapes. For imposter matching score, all the three train images of a user are matched with the ( $149 \times 2$ ) test images of another 149 users. The minimum of out of the three matches is stored as imposter score corresponding to each of the test user. Hence, for 150 users, 44700 ( $150 \times 149 \times 2$ ) are computed for both the vein patterns and hand-shapes.
- II. *The error rates:* These result from the comparison of both genuine and imposter scores against a threshold. The percentage of the rejected genuine matching scores by the decision-threshold is termed as false rejection rate (FRR) while the percentage of accepted imposter scores is termed as false acceptance rate (FAR). For a typical biometric authentication, the minimum FAR must be specified to get the corresponding genuine acceptance rate ( $\text{GAR} = 100 - \text{FRR}$ ).
- III. *The Receiver Operating Characteristics (ROC):* It is a plot of FAR Vs. GAR obtained by varying the threshold and finding FARs and GARs. In the conventional biometric systems, the threshold that yields the lowest FAR is selected from ROC. This threshold is used for making the decision of acceptance and rejection during the verification stage. We have used this curve to show the performance of the hand shape and the hand veins as individual biometric modalities. However, instead of ROC, our bimodal system employing the two traits uses ACO for the optimal selection of fusion parameters and decision threshold for each security level.
- IV. In our work, the selection of the optimal fusion parameters is largely dependent on the cost factor CFA; so the algorithm is run 100 times as in [25] for each value of CFA. The parameters that minimize G in Eq. (17) are varied along with CFA. However CFA is varied in the interval [0.1, 1.9]. The average and the standard deviation of the minimum error over 100 runs ( which is sufficient for all practical purposes) are needed since the average minimum error helps ascertain the performance of the bimodal system [25] [26] whereas the standard deviation of the minimum error helps to know the consistency of the algorithm [26].

The results of the bimodal system are discussed in the following order: First, the results of the score-level fusion using ACO; Second, comparison of ACO with PSO; and Third, comparison of the score-level fusion with the decision-level fusion.

*A. The Score-level Fusion using ACO*

The histograms of matching scores of the hand-shapes and hand-veins are shown in Fig. 11 (a)-(b) respectively. The ROCs of these modalities appear in Fig. 11 (c). The plots of the average and the standard deviation of the minimum error over 100 runs of the algorithm are shown in Fig. 12 (a) and (b) respectively. The average error of our bimodal system is significantly low as compared to that of the separate unimodal systems {Please see ROC curves in Fig. 11 (c)}. The standard deviation of the error is found as 0.0007 which shows that the ACO algorithm is stable over the 100 runs of algorithm. In order to see the suitability of the fusion rules, the probabilities of selection of each rule over 100 runs of the algorithm for each value of CFA are displayed in Fig. 13. From this, we can find that most of the times SUM rule and the PRODUCT rule are selected as the best fusion rule by the ants for most of the weights. However, SUM rule has shown slightly better performance over PRODUCT rule. As evident from the figure, PODUCT rule performs better than the SUM rule when CFA less than 0.5, though, at 0.3 the SUM rule performs better. At 0.6 both the rules have almost the same probability of selection. When CFA increases from 0.6, the SUM rule is selected with the highest probability implying high performance for the rest of the values of CFA.

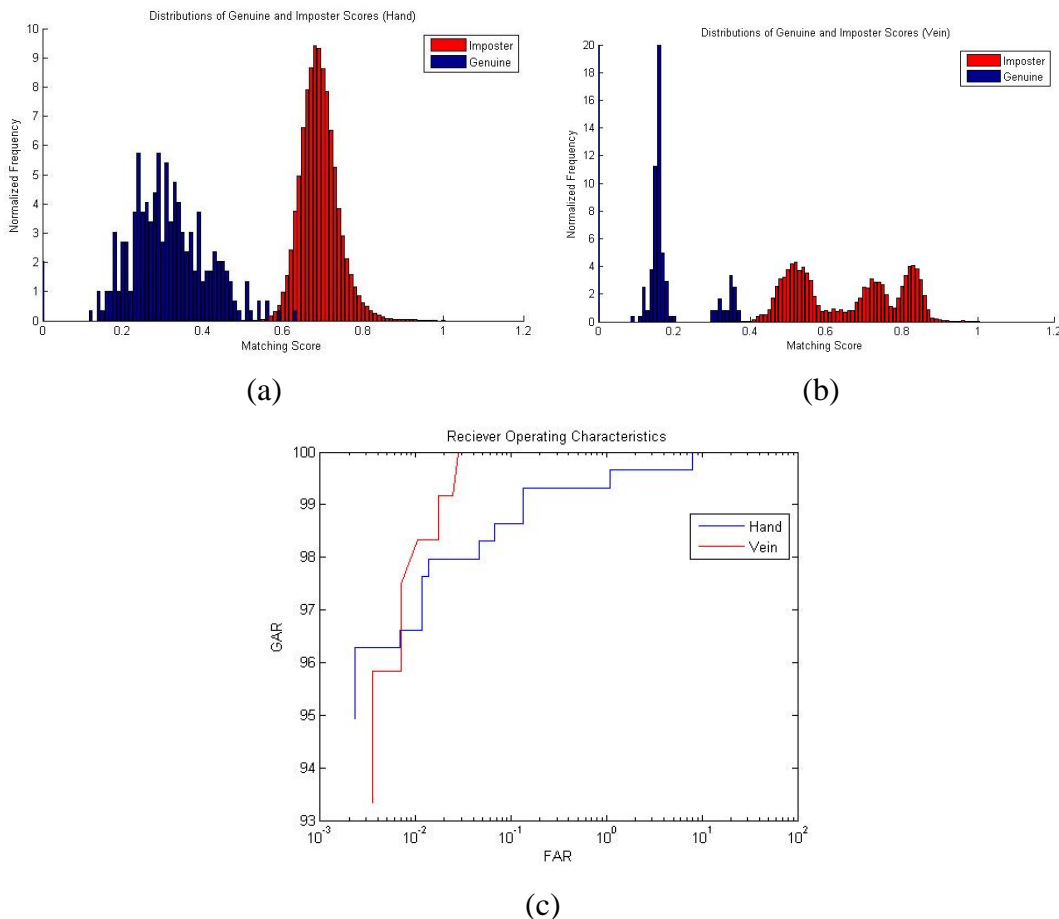


Fig. 11: (a) Histogram of the matching scores of the hand-shape (b) Histogram of the matching scores of vein patterns (c) Combined ROC curve for both

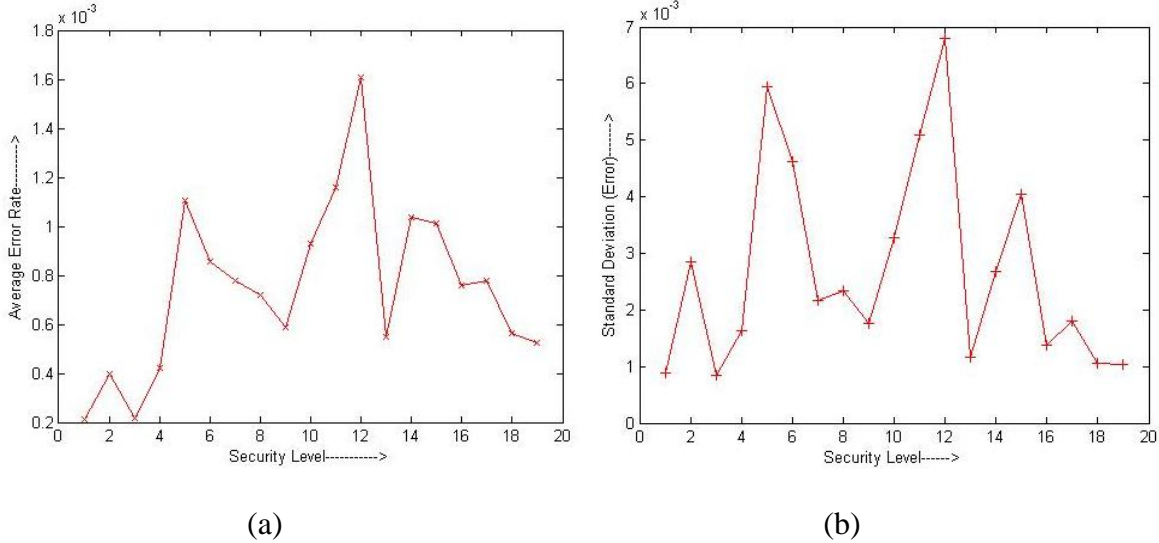


Fig.12: The plots of (a) the average of error (b) the standard deviation of error

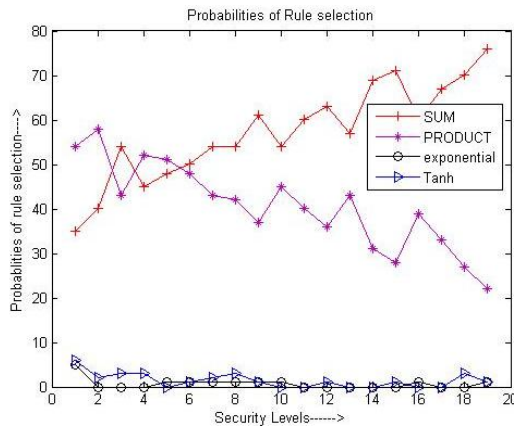


Fig. 13 Probabilities of the rule selection for each value of CFA

**B. Comparison of ACO with PSO**

PSO was used for the selection of fusion parameters in the previous works on the adaptive multimodal fusion [25]-[26]. In PSO, the parameters used are: inertia weight ( $W$ ) = 1.2, the social ( $\psi_1$ ) and the cognitive ( $\psi_2$ ) parameters are 1.2 and 0.9 respectively. The number of swarms is 15 whose initialization is the same as that of ants (See Section V-A) and 150 iterations are provided for getting a converged solution using PSO algorithm. The ACO Vs PSO plots of the average of error and the standard deviation of error are shown in Fig. 14 (a) and Fig. 14 (b) respectively for the score-level fusion. In both the plots, ACO-based selection of fusion parameters is found superior to that of PSO. The plot of the probabilities of rule selection for each CFA is shown in Fig. 14 (c). Unlike ACO, the probabilities of the selection of exponential and Tanh rules are higher with PSO.

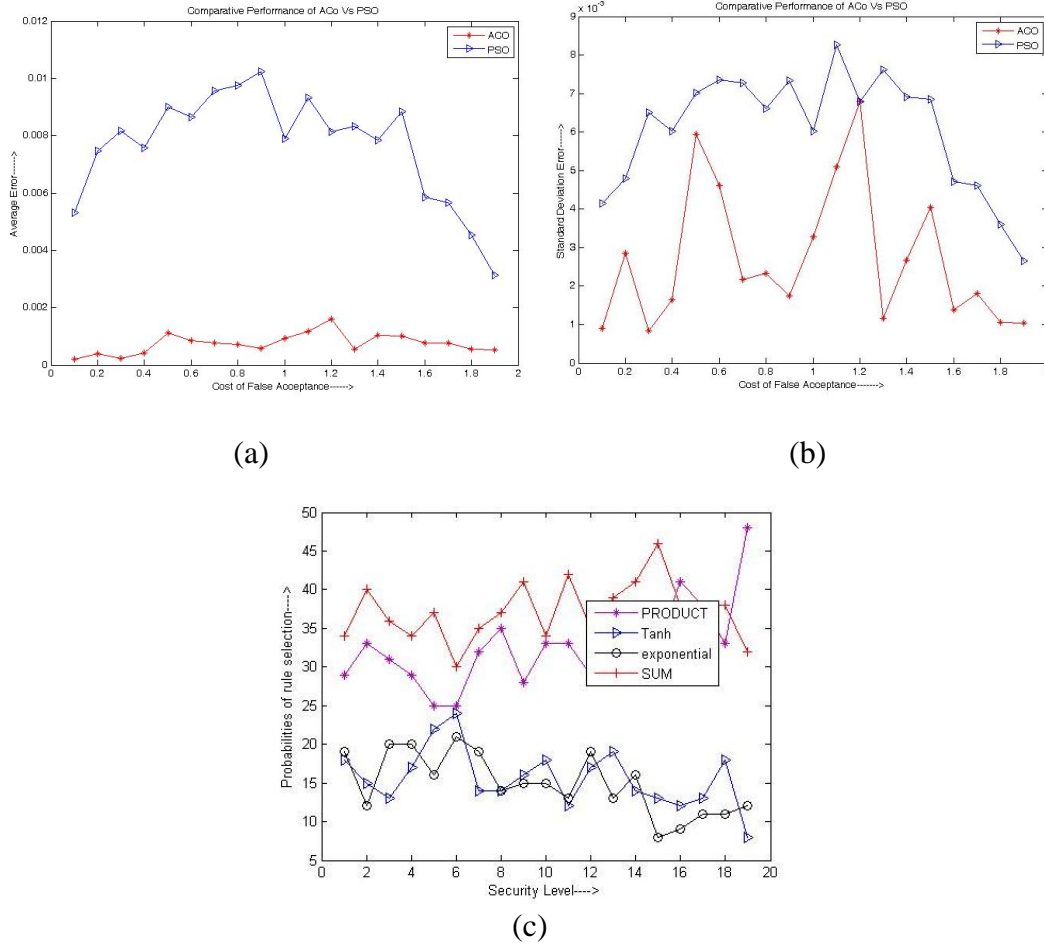


Fig.14: The plot of PSO Vs. ACO for the score-level fusion (a) The Average (b) The SD; (c) Rule selection using PSO

### C. Comparison of Score-level fusion with Decision-Level Fusion

The decision-level fusion strategy is employed in the PSO-based multimodal system first in [25] and then in [26]. However, the results of [26] indicate that the decision-level fusion scheme is inferior to the score-level fusion if the selection of fusion parameters is by PSO. Our study on the bimodal system reveals two points: (1) The decision-level fusion with ACO-based parameter selection is superior to the PSO-based selection, and (2) The score-level fusion is better than the decision-level fusion with ACO. As a verification of these points, see the plots of ACO Vs. PSO for the average error and the standard deviation of the error in Figs. 14(a)-(b) and Figs. 15 (a)-(b) respectively. To justify the first point, we note that ACO incurs less error in both the plots. Moreover, the differences of the average errors and of the SD errors between the ACO and PSO due to the score-level fusion (See Figs. 14a-b) are more than those due to the decision-level fusion {Fig. 15 (a)-(b)}. As regards the second point, see the average error for each value of CFA in Fig. 16 (a) and SD error for the same value of CFA in Fig. 16 (b). In both of the plots, score-level fusion gives low error rates than the decision-level.

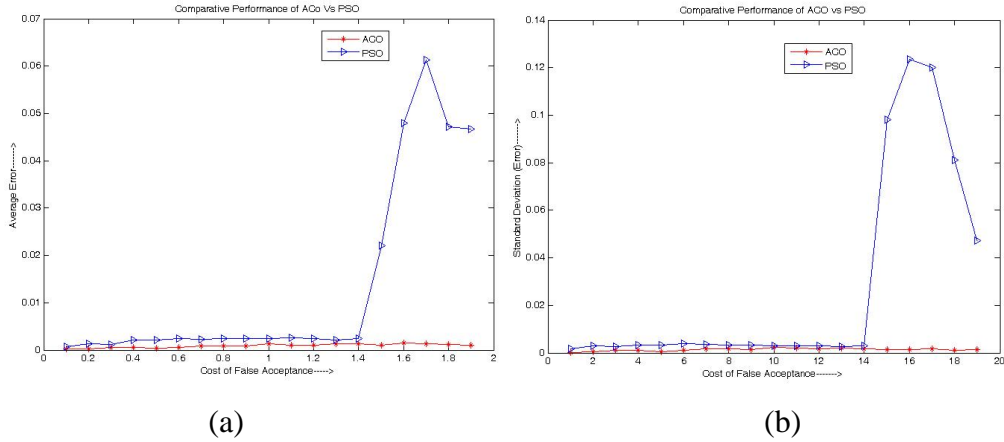


Fig.15 The plot of PSO Vs ACO for the decision-level fusion: (a) The Average (b) The SD

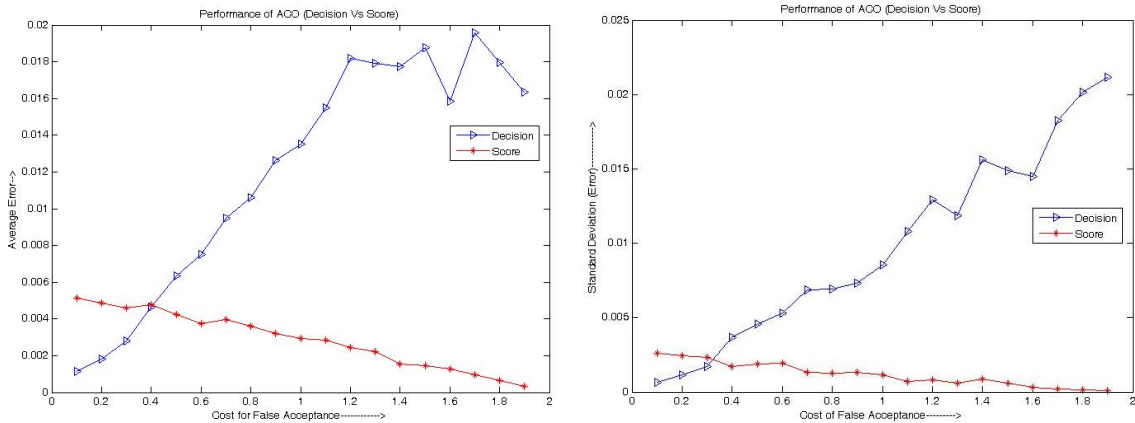


Fig. 16 The Performance of ACO on the Decision Vs. Score-level fusion (a) The Average (b) The SD

## VII. DISCUSSION

A survey on the biometric authentication shows diverse performance of biometric modalities based on application, availability, and user convenience. The eye-based biometrics like, iris or retina possesses high details and individuality. However, being a small and small target, irises are difficult to acquire with low user convenience. The face biometric has high user convenience and availability but it suffers from large pose and expression variations. The advantage with hand-based biometrics is that it possesses high textural details with high user convenience and availability. Though, people generally leave their handprints unconsciously by touching and chances of imposter attacks are much more in such scenario. Therefore, the recent trend in biometric literature is to investigate biometric modalities from the dorsal part of the hand which is acquired touch-less having lesser chances of imposter attacks.

Knuckle print is one such potential biometric modality recently developed with promising recognition rates. Kumar et al. [41] have achieved near 100% accuracy with FAR of 0.03%. Our earlier work [42] on knuckle print verification makes use of the fuzzy binary tree and ACO. Vein

patterns are another biometric modality that caught the attention of several researchers [10][30]-[31]. Hidden beneath the skin, vein patterns have lesser chances of imposter attacks and are shown to yield high recognition rates. Wang et al. [30] have shown 0% FAR and 0% FRR on infrared vein patterns. However, their experiments are conducted on a small database of only 30 users with 9 samples each. moreover, infrared thermal vein patterns need somewhat controlled environment at the time of acquisition along with proper management of imaging [30]. But once acquired correctly, they possess high textural details.

Our earlier works on unimodal [31] and bimodal [32] systems using hand vein patterns are encouraging. Though the hand vein patterns are less investigated, the bimodal system developed by integrating the vein patterns and hand-shapes is new. This work targets the indoor security applications and may be well suited for situations like *the access authentication for secret labs/building*. It is well known that when the user identity is known, verification is the most preferred mode for the personal authentication and some contributions in this mode are [8]-[10][13][25][26]. The case of identification is more suitable to the forensic and surveillance applications. However, in most of the civilian applications like building access problem or employee attendance system, a user can have his identity with him. The task of authentication in such cases is to verify the request of a claimed identity. A typical biometric system has therefore been designed by learning a suitable decision threshold which can reject an imposter attempt and at the same time accept a genuine attempt. The selection of an optimal decision threshold depends upon the expected security requirements which can be expressed in terms of the two error rates: false acceptance rate (FAR) or false rejection rate (FRR). The choice of acceptable error rates is application dependent (See Section *I-B*). The motivation for this work stems from the desire to design a bimodal system using infrared thermal hand veins and had shape by optimally selecting the decision parameters using ACO. It is noted that different security levels for different applications can be achieved using CFA/FFR (See Section *V-A*) and for each security level an optimal decision threshold, fusion rule, and weights for score level fusion {Eqn (18)-(21)} are computed using ACO (See Section *V-B*) in the proposed bimodal system. The computed decision thresholds can be utilized to distinguish a genuine attempt from an imposter attempt.

## VIII. CONCLUSIONS

This paper presents a novel bimodal system using infrared thermal hand-veins and visible hand-shape modalities. ACO is used to fuse these modalities at the score-level by learning the fusion parameters. Both traits can be simultaneously extracted from the user's hand, and the claimed identity is authenticated by integrating them. In order to make the proposed system adaptive to the varying security levels, ACO is used to select the fusion parameters according to the user defined cost functions. The experimental results indicate that for the varying security levels, the ACO-based selection of fusion parameters is well suited to the bimodal system as it fares well over PSO.

The experimental results carried out on the IITD database of 150 users demonstrate that the fusion parameters selected using ACO yield the lower values of the average error and the standard deviation error than those of the PSO. The main reason for the superior performance of ACO is that it avoids the premature convergence which in turn leads to near optimal selection of the fusion parameters most of the times. Further, ACO is defined for discrete domain and

therefore may be a better option than discrete variants of PSO like, binary PSO used in earlier systems.

The performance of the proposed bimodal system has the potential to authenticate reliably because of the internal structure of the vein patterns, that possess the properties such as uniqueness, stability and strong immunity against forgery, and the external structure of the hand-shape, which provide an effective appearance features. Thus our bimodal system is unique in the sense of capturing both internal and external structural information. As far as the implementation is concerned, our authentication system works on the computer with the configuration Core 2 Quad, 4 GB RAM using MATLAB 2009.

## REFERENCES

- [1] K. Jain, A. Ross, and S. Prabhakar, "An introduction to biometric recognition," *IEEE Trans. Circuits Syst. Video Technol.*, vol. 14, no. 1, pp. 4–20, Jan. 2004.
- [2] A.K. Jain, L. Hong and R. Bolle, "On-line Fingerprint Verification", *IEEE Transactions on PAMI*, Vol. 19, No. 4, pp. 302-314, 1997.
- [3] L. Hong, Y. Wan and A.K. Jain, "Fingerprint Image Enhancement: Algorithms and Performance Evaluation", *IEEE Transactions on PAMI*, Vol. 20, No. 8, pp.777-789, August 1998.
- [4] S. Pankanti, S. Prabhakar, and A. K. Jain, "On the Individuality of Fingerprints", *IEEE Transactions on PAMI*, Vol. 24, No. 8, pp. 1010-1025, 2002.
- [5] D. Zhang, W. K. Kong, J. You, and M. Wong, "Online palmprint identification," *IEEE Trans. Pattern Anal. Mach. Intell.*, vol. 25, no. 9, pp. 1041–1050, Sep. 2003.
- [6] J. You, W. Li, and D. Zhang, "Hierarchical palmprint identification via multiple feature extraction," *Pattern Recognition*, vol. 35, pp. 847-859, 2002.
- [7] A. K. Jain and J. Feng, "Latent Palmprint Matching", *IEEE Trans. PAMI* vol. 31, no. 6, pp. 1032-1047, June, 2009.
- [8] A. K. Jain and N. Duta, "Deformable matching of hand shapes for verification", *Proc. IEEE International Conference on Image Prcoessing*, October 25-28, Kobe, Japan, 1999.
- [9] A.K. Jain, A. Ross and S. Pankanti, "A Prototype Hand Geometry-based Verification System", *2nd Int'l Conference on Audio- and Video-based Biometric Person Authentication (AVBPA)*, Washington D.C., pp. 166-171, March 22-24, 1999.
- [10] Chih-Lung Lin, and Kuo-Chin Fan, "Biometric verification using thermal images of palm-dorsa vein patterns", *IEEE transactions on circuits and systems for video technology*, Vol. 14, pp. 199-213, 2004.
- [11] K. Nandakumar, "Integration of multiple cues in biometric systems", *PhD thesis*, Department of Computer Science & Engineering, Michigan State University, East Lansing, USA, 2005.
- [12] Available at: <http://www.dhs.gov/xlibrary/assets/CitizenGuidanceHSAS2.pdf>

- [13] A. Kumar, “Dynamic security management in multibiometrics,” in *Multibiometrics for Human Identification*, B. Bhanu and V. Govin-daraju, Eds. Cambridge, U.K.: Cambridge Univ. Press, 2010.
- [14] R. Horset and H. Tuy, “Global Optimization – Deterministic Approaches”, *Springer*, NewYork, 1996.
- [15] Noga Alon and Joel Spencer, “The Probabilistic Method”, *John Wiley*, June 2008 .
- [16] T. Bäck, D. Fogel and Z. Michalewicz, “Handbook of Evolutionary Computation”, IOP Publishing and Oxford University Press, New York, 1997.
- [17] J. Kennedy and R. C. Eberhart, “PSO optimization,” *Proc. IEEE Int. Conf. Neural Networks*, pp.1941–1948, 1995.
- [18] Kevin M Passino, “ Biomimicry of Bacteria Foraging for Distributed Optimization and control”, *IEEE Control Systems Magazine*, June 2002.
- [19] L. Hong and A. K. Jain, “Integrating faces and fingerprints for personal identification,” *IEEE Trans. Pattern Anal. Mach. Intell.*, vol. 20, no. 12, pp. 1295–1307, Dec. 1998.
- [20] R. Frischholz and U. Dieckmann, “BioID: A multimodal biometric identification system,” *Computer*, vol. 33, no. 2, pp. 64–68, Feb. 2000.
- [21] J. Fierrez-Aguilar, J. Ortega-Garcia, D. Garcia-Romero, and J. Gonzalez-Rodriguez, “A comparative evaluation of fusion strategies for multimodal biometric verification,” in *Proc. 4th Int. Conf. Audio- Video-Based Biometric Person Authentication*, J. Kittler and M. Nixon, Eds., 2003, vol. LNCS 2688, pp. 830–837.
- [22] A. Kumar, D. C. M. Wong, H. C. Shen<sup>1</sup>, and A. K. Jain, “Personal verification using palmprint and hand geometry biometric,” in *Proc. 4th Int. Conf. Audio- Video-Based Biometric Person Authentication*, J. Kittler and M. Nixon, Eds., 2003, vol. LNCS 2668, pp. 668–678.
- [23] Arun Ross, Anil Jain, “Information Fusion in Biometrics”, *Pattern Recognition Letters*, vol. 24 pp. 2115–2125, 2003.
- [24] A. K. Jain, K. Nandakumar, and A. Ross, “Score normalization in multimodal biometric systems,” *Pattern Recognit.*, vol. 38, no. 12, pp. 2270–2285, 2005.
- [25] Kalyan Veeramachaneni, Lisa Ann Osadciw, and Pramod K. Varshney, “An Adaptive Multimodal Biometric Management Algorithm”, *IEEE Trans. On Systems, Man, and Cybernetics—Part C: Applications and Reviews*, vol. 35, no. 3, August 2005.
- [26] Ajay Kumar, Vivek Kanhangad, and David Zhang, “A New Framework for Adaptive Multimodal Biometrics Management”, *IEEE Trans. on Information Forensics and Security*, Vol. 5, no. 1, pp. 92-102, March 2010.
- [27] E.S. Peer, F. mi de11 Bergll, A.P. Engelbrecht, “Using neighbourhoods with the guaranteed convergence PSO”, *IEEE Proceedings of Swarm Intelligence*, pp. 235-242, USA, April, 2003.
- [28] Genetic Algorithm, Available at: [http://en.wikipedia.org/wiki/Genetic\\_algorithm](http://en.wikipedia.org/wiki/Genetic_algorithm)

- [29] Y. Ding, D. Zhuang and K. Wang, "A study of hand vein recognition method," *Proc. IEEE Intl. Conf. Mechatronics & Automation*, Niagara Falls, Canada, pp. 2106 – 2110, Jul. 2005.
- [30] L. Wang, G. Leedham, and S.-Y. Cho, "Infrared imaging of hand vein patterns for biometric purposes", *IET Compt. Vis.*, Vol.1, pp. 113-122, 2007
- [31] Amioy Kumar, M. Hanmandlu and H. M. Gupta, "Online Biometric Authentication Using Hand Vein Patterns", *IEEE Symposium: Computational Intelligence for Security and Defense Applications*, Ottawa, Canada, 8-10 July 2009.
- [32] Amioy Kumar, Madasu Hanmandlu, Harsh Sanghvi, H. M. Gupta, "Decision level biometric fusion using Ant Colony Optimization", *In Proceedings of ICIP*, pp.3105-3108, HongKong, Sept. 2010.
- [33] De-Shuang Huang , Wei Jia, David Zhang, " Palmprint verification based on principal lines", *Pattern Recognition*, Vol. 41, pp. 1316 – 1328, 2008.
- [34] Erdem Yoruk, Ender Konukoglu, and Bulent Sankur, "Shape-Based Hand Recognition", *IEEE Transactions On Image Processing*, Vol. 15, No. 7, JULY 2006.
- [35] D. R. Kisku, P. Gupta, J. K. Sing, and C. J. Hwang, "Multispectral Palm Image Fusion for Biometric Authentication using Ant Colony Optimization", *IEEE 1st International Workshop on Emerging Techniques and Challenges for Hand-based Biometrics (ETCHB 2010)*, pp. 1-7, Istanbul, Turkey, August 2010.
- [36] H. R. Kanan, K. Faez, M. Hosseinzadeh, "Face Recognition System Using Ant Colony Optimization-Based Selected Features", *IEEE Symposium on CISDA*, PP. 57-62, 1-5 April 2007.
- [37] F. Matus, J. Flusser, "Image representations via a finite Radon transform", *IEEE Trans. Pattern Anal. Mach. Intell.* 15 (10) (1993) 996–1006.
- [38] Marian Stewart Bartlett, Javier R. Movellan ,and Terrence J. Sejnowski, "Face Recognition by Independent Component Analysis", *IEEE Transactions on Neural Networks*, Vol. 13, No. 6, November 2002.
- [39] A. Hyvarinen and E. Oja, "Independent component analysis: algorithms and applications," *Neural Netw.*, vol. 13, no. 4–5, pp. 411–430, 2000.
- [40] Dorigo M., G. Di Caro and L. M. Gambardella "Ant Colony System: A Cooperative Learning Approach to the Traveling Salesman Problem" *IEEE transactions on evolutionary computation*, vol. 1, no. 1, April 1997.
- [41] Ajay Kumar, Yingbo Zhou, "Personal Identification using Finger Knuckle Orientation Features", *Electronics Letters*, vol. 45, no. 20, September 2009.
- [42] A. Kumar, M. Hanmandlu, and H. M. Gupta, "Ant colony optimization based fuzzy binary decision tree for bimodal hand knuckle verification system", *Expert Systems with Applications*, 2012, HU<http://dx.doi.org/10.1016/j.eswa.2012.07.042>UH. {In the Press}.
- [43] A.C. Copeland, G. Ravichandran, M.M. Trivedi, Localized radon transform-based detection of ship wakes in SAR images, *IEEE Trans. Geosci. Remote Sensing* 33 (1) (1995) 35–45.

- [44] T. Pavlidis, *Algorithms for Graphics and Image Processing*, Computer Science Press, Rockville, Maryland, 1982.